High-brightness green InP-based QLEDs enabled by *in-situ* passivating core surface with zinc myristate

To cite this article: Yuanbin Cheng *et al* 2024 *Mater. Futures* **3** 025201

View the article online for updates and enhancements.

High-brightness green InP-based QLEDs enabled by *in-situ* passivating core surface with zinc myristate

Yuanbin Cheng[1], Qian Li[1], Mengyuan Chen, Fei Chen*[ID], Zhenghui Wu*[ID] and Huaibin Shen

Key Laboratory for Special Functional Materials of Ministry of Education, National & Local Joint Engineering Research Center for High-efficiency Display and Lighting Technology, Henan University, Kaifeng 475004, People's Republic of China

E-mail: chenfei.henu@henu.edu.cn and wuzhenghuihk@henu.edu.cn

CrossMark

Abstract

The performance of red InP and blue ZnTeSe-based quantum dots (QDs) and corresponding QD light emitting diodes (QLEDs) has already been improved significantly, whose external quantum efficiencies (EQEs) and luminances have exceeded 20% and 80 000 cd m^{-2}, respectively. However, the inferior performance of the green InP-based device hinders the commercialization of full-color Cd-free QLED technology. The ease of oxidation of the highly reactive InP cores leads to high non-radiative recombination and poor photoluminescence quantum yield (PL QY) of the InP-based core/shell QDs, limiting the performance of the relevant QLEDs. Here, we proposed a fluoride-free synthesis strategy to *in-situ* passivate the InP cores, in which zinc myristate reacted with phosphine dangling bonds to form Zn–P protective layer and protect InP cores from the water and oxygen in the environment. The resultant InP/ZnSe/ZnS core/shell QDs demonstrated a high PL QY of 91%. The corresponding green-emitting electroluminescence devices exhibited a maximum EQE of 12.74%, along with a luminance of over 175 000 cd m^{-2} and a long T_{50}@100 cd m^{-2} lifetime of over 20 000 h.

Supplementary material for this article is available online

1. Introduction

Due to cadmium's toxicity and carcinogenic effects, InP based quantum dots (QDs) are the material most favored for new QD displays [1–10]. By changing size, their spectra can cover the entire visible region. However, compared with Cd-based QDs, InP-based QDs tend to have lower photoluminescence quantum yields (PL QYs) and broader full-width at half-maximum (FWHM). In particular, bare InP core has extremely low PL QY ($<1\%$) due to the ease of oxidation of their highly reactive surface even in insert reaction chambers. It has been reported that the defects from oxidative species are probably the reasons for the non-radiative recombination and poor PL QY of InP-based core/shell QDs [11–14]. Therefore, eliminating the surface defects to improve the optoelectronic properties of InP-based QDs is critical to incentivizing the transition to less toxic QD materials.

Over the past decade, extensive studies have been applied to improve the optoelectronic properties of InP-based QDs for display and lighting applications [9, 10, 14–20]. The most common method is growing shells composed of wide-bandgap semiconductors (ZnS, ZnSe, ZnSeS) on InP cores [21–24]. The shell composition and structure have been carefully optimized to reduce defects and improve radiative recombination. However, the surface defects still exist even after the shell growth. Therefore, eliminating surface defect states of the InP core before and during the shell coating is necessary to enhance the optoelectronic characteristics of core/shell QDs. So far, the most widespread and effective method for synthesizing InP-based QD with PL QY as high as 90% for consumer displays is the addition of hydrofluoric acid (HF) before shell growth [25–28]. The introduction of fluoride ions not only can eliminate surface oxides, but also passivate the dangling bonds around phosphorus atoms and fill the vacancies on the InP core. Nevertheless, HF has severe toxicity and corrosivity, which makes it unsuitable for large-scale synthesis. Hence, Li *et al* reported red InP/ZnSe/ZnS core/shell QDs with a near-unity PL QY by treated with inorganic salt ZnF_2. The corresponding QD light emitting diodes (QLEDs) achieved a maximum external quantum efficiency (EQE) of 22.2% and a peak luminance of over $110\,000$ cd m^{-2}. Particularly, the device showed a T_{95} lifetime of over $32\,000$ h. This strategy has shown the highest efficiency in electroluminescence devices to date [14]. However, the generation of HF at high temperature can rapidly increase the pressure in the container, posing a concealed risk. Therefore, a safe and easy synthesis strategy is necessary for growing high-quality InP-based QDs.

Here, we demonstrate a fluoride-free synthesis strategy in which zinc myristate reacts with phosphine dangling bond to form Zn–P protective layer and protect InP core from environmental influences. Eventually, it enhances the optoelectronic properties of the cores and the corresponding core/shell structures. X-ray photoelectron spectroscopy (XPS) tests suggested the efficient removal of defects. The resultant InP/ZnSe/ZnS core/shell QDs exhibit a PL peak of 534 nm, an average size of 8.1 nm and a high PL QY of 91%. The corresponding green-emitting electroluminescence device demonstrates a high EQE of 12.74% and a peak current efficiency of 53.31 cd A^{-1}. Especially, the device obtains a luminance of over $175\,000$ cd m^{-2} and a long $T_{50}@100$ cd m^{-2} (which characterizes how long it takes for the 100 cd m^{-2} luminance to decrease to its half) lifetime of over $20\,000$ h. As we know, the luminance is the state-of-the-art value among those for the reported green InP-based QLEDs.

2. Method

2.1. Synthesis of InP/ZnSe*thin* cores

To synthesize the green InP cores, 0.2 mmol $In(Ac)_3$, 0.1 mmol $Zn(Ac)_2$, 0.8 mmol MA, and 10 mL of ODE were mixed and placed in a 50 mL flask, and then degassed at 150 °C for 30 min. Then, phosphorus precursors were promptly injected into the above mixture under nitrogen atmosphere, and the mixture was heated to 270 °C to grow InP cores for 3 min. In turn, 1 mL $ZnMy_2$ was added at this temperature and reacted for 5 min. Then, 1 mL Se-ODE was injected and kept for 15 min at 270 °C. After completion, the reaction dropped to room temperature. The cooled solution was purified one time using hexane and ethanol, and then redispersed into hexane for shell coating.

2.2. Synthesis of the InP/ZnSe/ZnS core/shell QDs

The InP/ZnSe*thin* cores, 2 mmol $Zn(St)_2$, 0.55 mmol $Zn(Ac)_2$ and 10 mL ODE were mixed and placed in a 50 mL flask, followed by degassing at 150 °C for 10 min, and then 1 mL Se-ODE was added with increasing reaction temperature to 200 °C. For the ZnSe shell growth, the 0.5 mL Se-ODE was added every 10 min, and the mixture was heated to 310 °C at each 10 °C. The Se-ODE maintained a total addition of 10 mL. Then, we cooled the mixture down to room temperature. Following, for further ZnSe shell growth, 2 mmol $Zn(St)_2$ and 0.55 mmol $Zn(Ac)_2$ were added to the mixture, and then raised the reaction temperature to 310 °C. Furthermore, the 0.5 mL Se-ODE was added every 10 min until the total additional amount was 15 mL. Finally, the ZnS shell was grown by adding 0.5 mL S-ODE-TOP every 10 min three times. The cooled solution was purified by hexane and ethanol three times, and then redispersed into n-octane.

2.3. Preparation of ZnMgO nanoparticle (NC)

$Mg(OAc)_2 \cdot 4H_2O$ and $Zn(OAc)_2 \cdot 2H_2O$ with a ratio of 1:7 by mass were dissolved in DMSO to form 15 mL solution at a concentration of 0.50 mol L^{-1}. TMAH was dissolved in ethanol to form 5 mL solution with a concentration of 0.55 mol L^{-1}. Then, the above two solutions were mixed and then stirred for 1 h. Finally, the solution was purified by n-hexane and redispersed in ethanol. The concentration of ZnMgO NC was maintained at 30 mg mL^{-1}.

3. Results

In the synthesis, myristic acid, indium acetate and ODE were mixed in a 100 mL flask. Then, the $(TMS)_3P$ precursors were injected quickly at 150 °C under nitrogen atmosphere and maintained for 3 min to promote the InP core growth. However, the extreme reactivity of $(TMS)_3P$ would lead to the fast depletion of $(TMS)_3P$ in solution, which seriously affected the subsequent growth process of InP core. Herein, we added $ZnMy_2$ at 270 °C and adjusted its concentration (figure S1, supporting information), which could adjust the nucleation and eliminate surface oxidation. Choi *et al* reported that the introduction of $ZnMy_2$ might produce Zn–P complex, which acted as phosphine reservoir to improve the monodisperse in the growth process [29]. As shown in figure 1(a), compared with the InP cores without $ZnMy_2$, the InP cores with $ZnMy_2$ have an increased absorption valley/peak ratio (Vd) of 0.5 and a narrower FWHM of 35 nm, indicating their more uniform size distribution. What is more, the InP core with
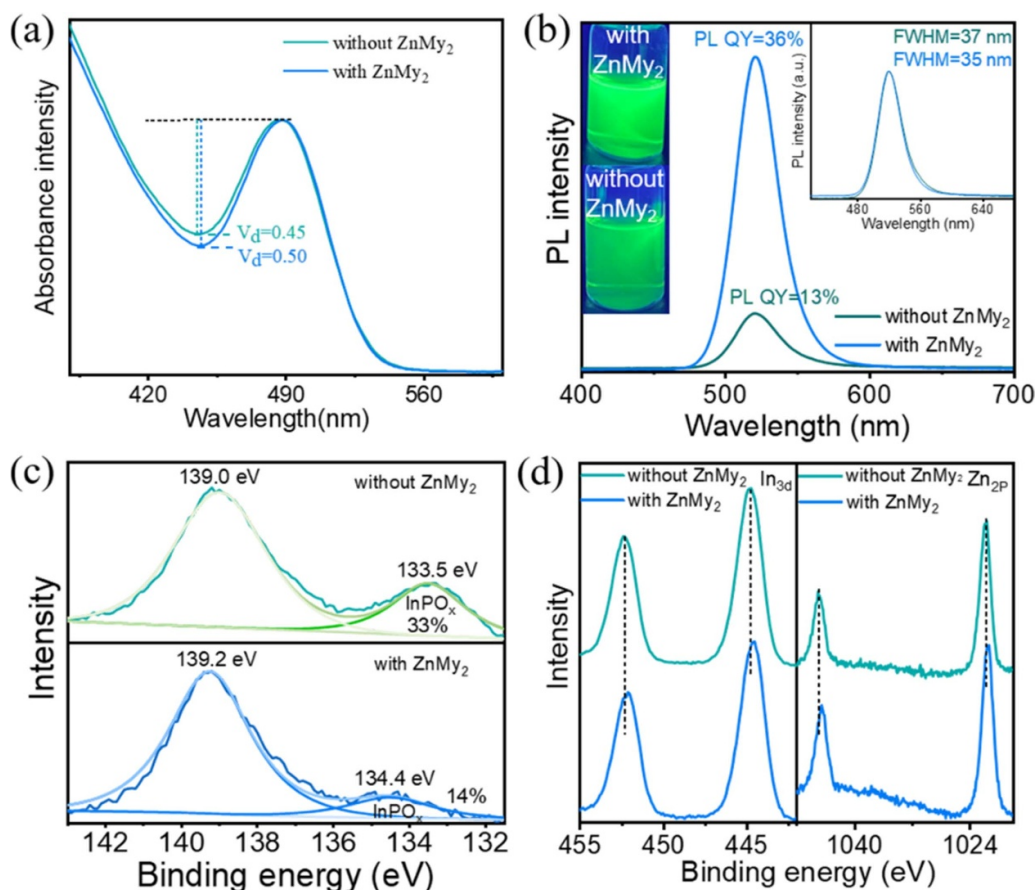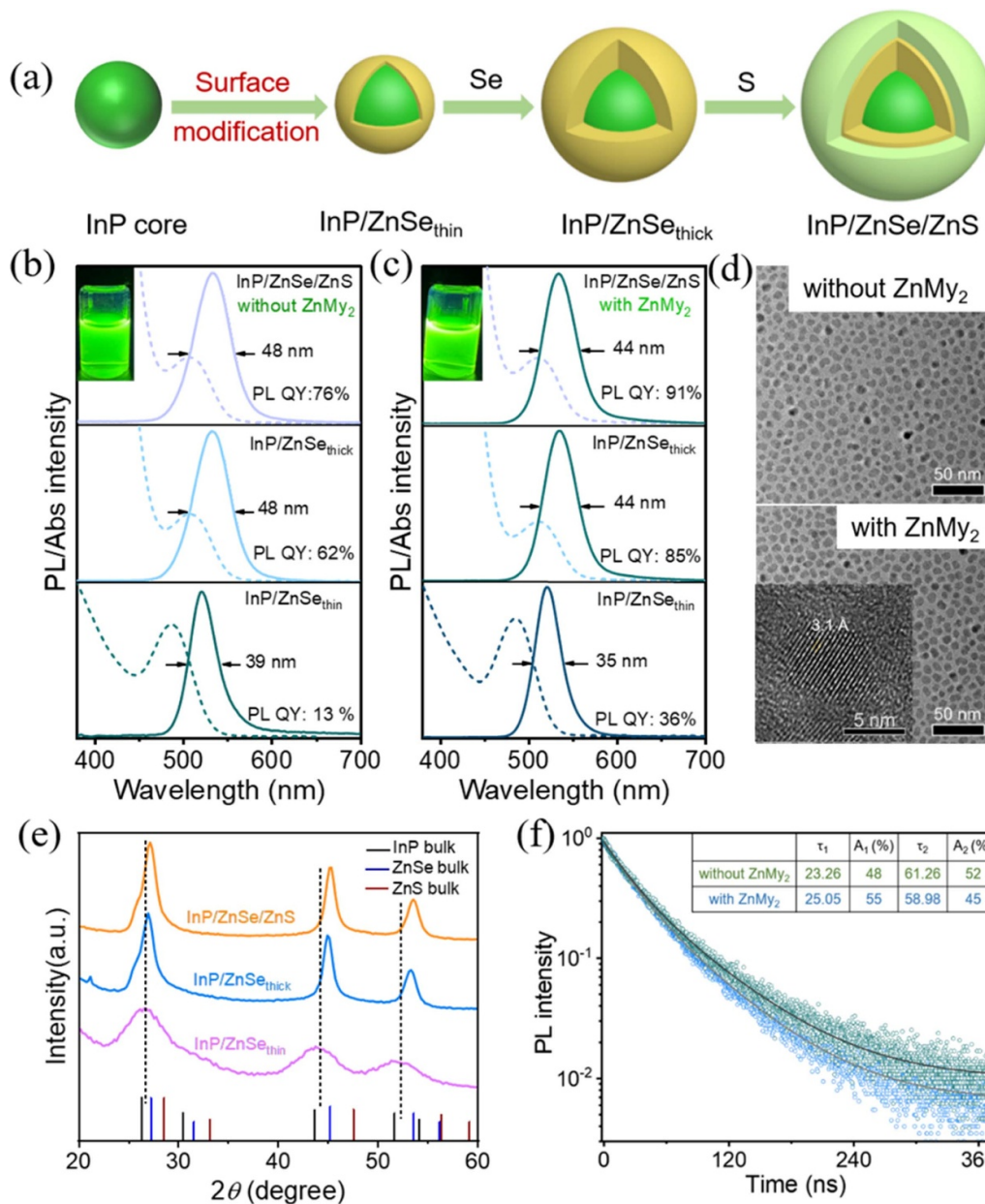
Figure 1. (a) UV–vis absorption and (b) PL spectra of InP cores without and with $ZnMy_2$. High-resolution XPS signals of (c) P spectra and (d) In and Zn spectra for InP cores without and with $ZnMy_2$. The inset in figure 1(b) shows photographs of the InP cores without (bottom) and with $ZnMy_2$ (top) solution under UV irradiation.

$ZnMy_2$ exhibits brighter green light emission even without shell formation (figure 1(b)). Correspondingly, the PL QY increases from 13% for the InP core without $ZnMy_2$ to 36% for the InP core with $ZnMy_2$. From the inset of figure 1(b), we can see the tailing emission in the InP core without $ZnMy_2$, which may be attributed to their surface defect states caused by oxidation. To verify this hypothesis, XPS spectra were also analyzed (figure 1(c)). In the XPS spectra for P2p, the peak near 133.5 eV is attributed to the oxidized phosphorus due to the formation of P–O bond. The area ratio of P–O decreases from 33% for the InP core without $ZnMy_2$ to 14% for that with $ZnMy_2$, indicating that $ZnMy_2$ can react with the surface of InP core and inhibit the development of the InPOx surface oxide layer. In order to further analyze the interaction between $ZnMy_2$ and the surface of InP core, high-resolution XPS signals of In3d and Zn2p spectra were tested. As shown in figure 1(d), due to the weaker electronegativity of P than that of Se, the peak of Zn2p shifts to lower energy by 0.4–0.6 eV when the Zn–Se bond is partially replaced by Zn–P complex. ^{1}H NMR spectra (figure S2 in supporting information) also supported that Zn atoms from $ZnMy_2$ were transferred to the vicinity of phosphine atoms and formed Zn–P complex. The signal around 2.20–2.25 ppm in ^{1}H NMR spectra corresponds to the –CH_2– around the carboxy group in myristic acid. The ^{1}H NMR spectra of $ZnMy_2$ did not show any peaks

around 2.20–2.25 ppm, since there was no carboxy group. However, the peaks around 2.20–2.25 ppm appear again after mixing $ZnMy_2$ and phosphine precursor, which indicates that Zn atoms were removed from $ZnMy_2$ and a small amount of myristic acid was obtained. The free Zn^{2+} ions combined with phosphine atoms to form Zn–P complex. In addition, the ^{1}H NMR signal of phosphine in 0.89–0.93 ppm shifted to the left after it mixed with $ZnMy_2$ and formed Zn–P complex. This meant that the valence state of H atoms became less positive and that of phosphine atoms became less negative in $(TMS)_3P$, leading to a less chemical reactivity of phosphine precursor. The formation of Zn–P complex will protect the InP core from the influence of water and oxygen in the environment, while it improves the monodisperse through the phosphine reservoir on the other hand. The peak of In_{3d} shifted to lower energy by 0.3 eV, which further verified the reduction of $InPO_x$.

What is more, the quasi-ZnSe shell was introduced to avoid the InP core Ostwald ripening at high temperature [30]. As can be seen from figure S3 in supporting information, the exciton peak position of the InP core with $ZnMy_2$ in absorption spectra is red-shifted by 30 nm, indicating that the size of InP/ZnSe_thin with $ZnMy_2$ is larger. The corresponding TEM images (figure S4, supporting information) also verified this conclusion, and the average size of the cores is 2.8 nm (with $ZnMy_2$) and 2.0 nm (without $ZnMy_2$), respectively. The above

Figure 2. (a) Synthetic route of InP/ZnSe/ZnS QDs. Absorption and PL spectra of InP/ZnSe/ZnS QDs (b) without and (c) with ZnMy$_2$. The photographs of both the QDs solutions under UV irradiation are shown in the insets. (d) TEM pictures of InP/ZnSe/ZnS QDs without (top) and with ZnMy$_2$ (bottom). (e) XRD patterns of InP/ZnSe$_{thin}$, InP/ZnSe and InP/ZnSe/ZnS QDs. (f) Time-resolved PL decays of InP/ZnSe/ZnS QDs without and with ZnMy$_2$.

results show that the ZnMy$_2$ is degraded to form Zn^{2+} and myristic acid after mixing. Zn^{2+} combine with phosphine to form Zn–P complex, while myristic acid enters the solvent. When Se-ODE is added, Zn in Zn–P complex can act as a Zn source, forming a thin ZnSe shell layer. Furthermore, the Zn–P complex can also act as phosphine reservoir to control the monodisperse growth process, and act as a protective layer to avoid the exposure of InP core to water and oxygen. Therefore, the more uniform size distribution and better surface passivation of InP cores will bring about improved PL QY, which are also beneficial for subsequent shell growth.

Subsequently, we coated the ZnMy$_2$-treated InP core with ZnSe/ZnS shell and studied the effect of ZnMy$_2$ addition on

shell growth. Figure 2(a) displays the route for synthesizing InP/ZnSe core/shell QDs and InP/ZnSe/ZnS core/shell/shell QDs. The evolution of spectra and morphologies are shown in figures 2(b)–(d), respectively. Both samples show red shifts of the first excitonic absorption and the PL peaks after ZnSe coating. This is because the offset between the conduction bands of InP core and ZnSe inner shell is small. To further grow the ZnS outer shell, electrons are well confined because there is a larger band offset between ZnS and InP, limiting the shift of emission peaks. Finally, InP/ZnSe/ZnS QDs were synthesized with a similar PL peak located at 534 nm. As verified by TEM in figure 2(d), the average size for the as-prepared core/shell/shell QD with ZnMy$_2$ is estimated to be 8.1 ± 1.0 nm with better
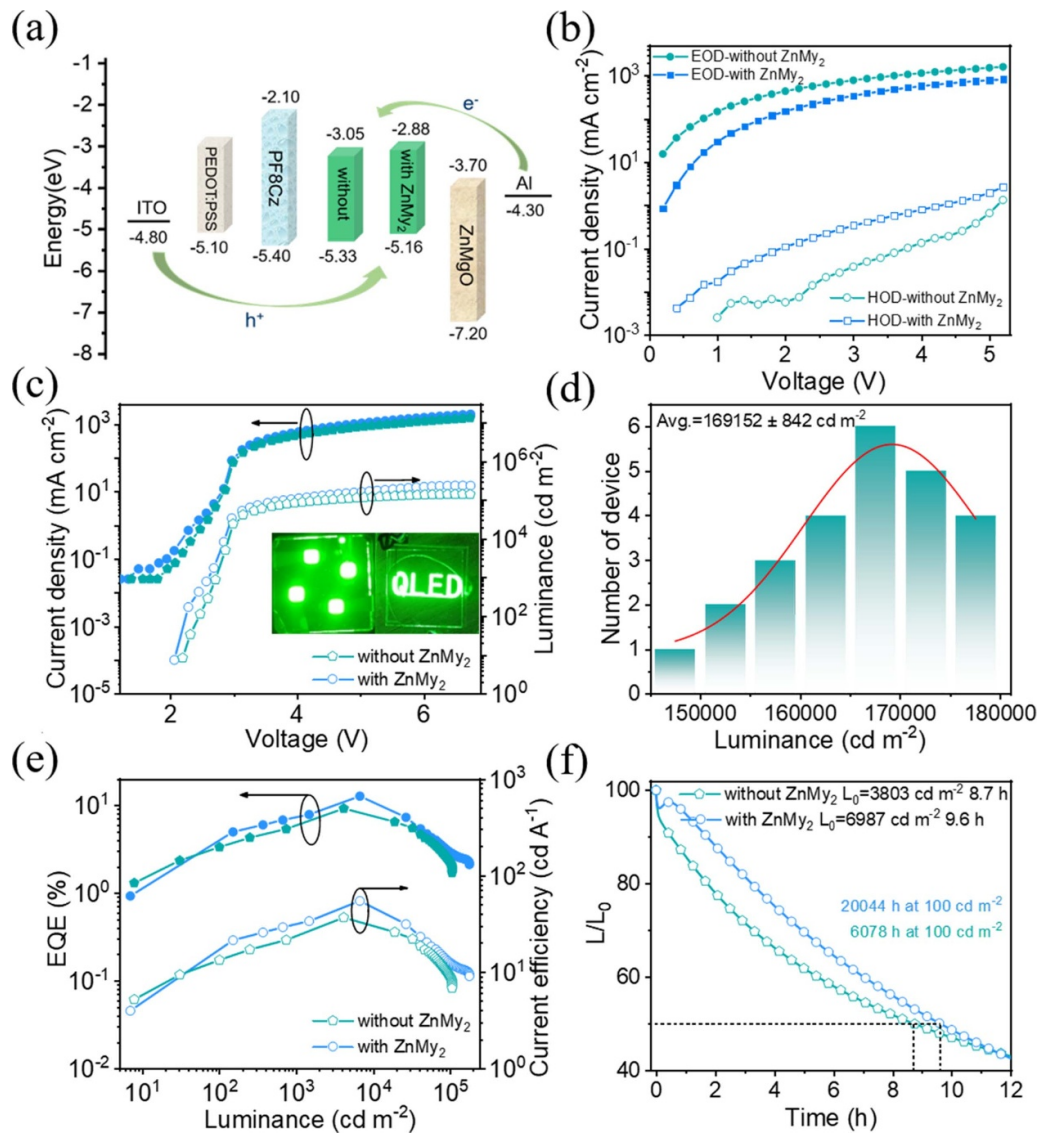
Figure 3. (a) The energy levels of QLEDs (Its structure is ITO/PEDOT:PSS/PF8Cz/QD/ZnMgO/Al). (b) The current density–voltage (*J*–*V*) characteristics of hole-only-device (HOD: ITO/PEDOT:PSS/PF8Cz/QD/MoO$_3$/Al) and electron-only-device (EOD: ITO/ZnMgO/QD/ZnMgO/Al). (c) The curves of current density and luminance with voltage variation for the device without and with ZnMy$_2$. (d) The histogram distribution of luminance for 25 devices treated with ZnMy$_2$. (e) The curves of EQE and current efficiency with luminance variation for the QLEDs without and with ZnMy$_2$. (f) The operational lifetimes of QLEDs without and with ZnMy$_2$.

size distribution, while the average size for the QD without ZnMy$_2$ is smaller (7.8 ± 1.2 nm) (figures S5(a) and (b), supporting information). The better size distribution might be attributed to the more uniform effective growth of the shell layer due to the minor defects in the InP/ZnSe$_{thin}$ cores. QDs with ZnMy$_2$ show high crystallinity as suggested by the high-resolution transmission electron microscopy image. The (111) plane shows a lattice spacing of ∼0.31 nm (inset), confirming that the ZnS outer shell is epitaxially grown successfully. This result is consistent with the x-ray diffraction (XRD) patterns, as shown in figure 2(e). The three peaks at 26.6°, 44.2°, and 52.2° in the XRD patterns correspond to (111), (220), and (311) planes, respectively, which indicates that the InP core is a zinc-blende crystal structure. Continue to grow the ZnSe inner shell and ZnS outer shells, the three peaks are moved to higher angles and gradually become narrower, indicating the

successful growth of ZnSe and ZnS shells. What's more, the addition of ZnMy$_2$ has almost no effect on the lattice structure of QD (figure S5(c), supporting information). By virtue of the passivation of the core, the core/shell QDs with ZnMy$_2$ demonstrate an improved optical property with a high PLQY of 91% and an FWHM of 44 nm. In contrast, the relatively low PL QY (76%) and broadened emission (48 nm) of QDs without ZnMy$_2$ can be ascribed to the imperfect passivation of defect states in the InP/ZnSe$_{thin}$ core. The PL decays of both samples are shown in figure 2(f). The time-resolved PL decays is fitted with a double exponential, where A_1 (A_2) and τ_1 (τ_2) are the fraction ratios and lifetimes of the exciton (trapped exciton) emissions [31, 32]. The exciton emissions not only have increased PL lifetime (form 23.26 ns to 25.05 ns) but also have increased fraction ratios (from 48% to 55%), while the PL lifetime of trapped exciton emissions decreased from 61.26 ns

Table 1. Summary of turn-on voltage (V_{on}), EQE, current efficiency (η_A), maximum luminance (L_{max}) and lifetime of our QLEDs.

	V_{on} (V)	EQE (%)	η_A (cd A^{-1})	Luminance (cd m^{-2})	T_{50} lifetime (h)@100 cd m^{-2}
Without ZnMy$_2$	2.2	9.22	36.72	105 127	6078
With ZnMy$_2$	2.0	12.74	54.56	175 084	20 044

to 58.98 ns with the introduction of ZnMy$_2$. The average PL lifetime of QDs solution without ZnMy$_2$ is 43.02 ns, while the lifetime of ZnMy$_2$-treated InP QDs decreases to 40.32 ns. The above result suggests that the treatment of ZnMy$_2$ not only can reduce the exciton quenching, but also can enhance the radiative recombination rate.

We next fabricated QLEDs with the benchmark structure of ITO/PEDOT:PSS/PF8Cz/QDs/ZMO/Al using InP/ZnSe/ZnS QDs as the emitting layer (figure 3(a)). They exhibit a bright green color, and their Commission Internationale de l'Eclairage chromaticity coordinates are (0.304, 0.675) (figure S6, supporting information). The fabrication process of QLEDs is detailed in the supporting information. The energy levels of the charge transport layer were acquired from literature [33–35], and the energy level of QDs was calculated through a combination of ultraviolet photoelectron spectroscopy and optical measurements. As can be seen from figure S7 in supporting information, according to the formula of work function = 21.22-cutoff edge of secondary electrons, the valence bands of QDs without and with ZnMy$_2$ are 5.33 eV and 5.16 eV, respectively. Taking the similar bandgap of the two QDs (2.28 eV) into account, their conduction bands are 3.05 eV and 2.88 eV, respectively. The upward shift of the valence band and conduction band not only facilitates hole injection but also suppresses the injection of electrons, thereby facilitating the radiative recombination of injected charge carriers. To verify the conclusion, we fabricated the hole-only-device (HOD: ITO/PEDOT:PSS/TFB/QDs/MoO$_3$/Al) and the electron-only-device (EOD: ITO/ZMO/QDs/ZMO/Al) (see figure S8 in supporting information for the diagrams of energy level), and the *J–V* curves are exhibited in figure 3(b). The QLEDs with ZnMy$_2$-treated QDs show improved hole injection and decreased electron injection at any voltages, indicating more balanced charge injection and more effective radiative recombination of injected carriers. As can be seen from figure S9 in supporting information, the result was confirmed further by capacitance–voltage curves. The device with ZnMy$_2$ has smaller peak capacitances than that of the device without ZnMy$_2$, suggesting reduced charge accumulations and more effective radiative recombination.

The *J–L–V* characteristics of the devices without and with ZnMy$_2$ are demonstrated in figure 3(c). The device with ZnMy$_2$ exhibits a smaller turn-on voltage (2.0 V) than that of the device without ZnMy$_2$ (2.2 V), which may be related to the improved hole injection. In addition, with only a slightly larger current density (around 20% larger), the QLED based on ZnMy$_2$-treated QDs shows much higher luminance within the entire voltage range, and the peak luminance reaches 175 084 cd m^{-2}, which is improved by 67% compared to the device without ZnMy$_2$ (105 127 cd m^{-2}). As far as we know, the luminance is the state-of-the-art value among those

of the previously reported green InP-based QLEDs [36, 37]. Importantly, devices can achieve high brightness even at lower voltages (e.g. 26 321 cd m^{-2}@ 3.0 V and 83 834 cd m^{-2}@ 4.0 V), which is beneficial for the reduction of joule heat, thereby improving the device stability. The histogram of the luminance of 25 devices indicates excellent fabrication reproducibility (figure 3(d)), and an average luminance of over 169 152 ± 842 cd m^{-2}. The dramatically higher luminance but just slightly larger current density in the device with ZnMy$_2$ means more effective radiative recombination efficiency of carriers. According to the EQE-current efficiency-luminance characteristics in figure 3(e), the peak EQE and current efficiency reach 12.74% and 54.56 cd A^{-1} at the luminance of 6643 cd m^{-2} for the device with ZnMy$_2$, which is more than 38% higher than the maximum EQE of 9.22% and current efficiency of 36.72 cd A^{-1} for the QLEDs without ZnMy$_2$. Finally, we compare the T_{50} lifetimes of the QLEDs with and without ZnMy$_2$-treated QDs (figure 3(f)). When the initial luminance is 6987 cd m^{-2}, the device with ZnMy$_2$-treated QDs obtains a T_{50} lifetime of 9.6 h. According to the formula $L_0{}^n T_{50}$ = constant (L_0: initial luminance, n: acceleration factor, T_{50}: half lifetime), the T_{50}@100 cd m^{-2} lifetime of QLEDs with ZnMy$_2$-treated QDs is calculated to be 20 044 h with $n = 1.80$. However, the T_{50}@100 cd m^{-2} was only about 6078 h for the QLEDs without ZnMy$_2$. The device performance is also shown in table 1.

4. Conclusion

In summary, by *in-situ* passivating the InP core with ZnMy$_2$, the resultant InP/ZnSe/ZnS QDs exhibit a PL peak of 534 nm and a high PL QY of 91%. Additionally, the corresponding green-emitting QLEDs show enhanced performance with an EQE of 12.74%, a peak current efficiency of 53.31 cd A^{-1}, along with a breakthrough luminance of 175 084 cd m^{-2} and a long T_{50}@100 cd m^{-2} lifetime of more than 20 000 h. The XPS and ^{1}H NMR spectra demonstrated that the introduction of ZnMy$_2$ not only acts as phosphine reservoir to control the monodisperse growth process, but also acts as a protective layer to protect the InP core from being affected by the water and oxygen in the environment.

5. Future perspectives

With the acceleration of the commercialization of QDs in terms of display and lighting, the performance enhancement of environmentally friendly QDs and corresponding electroluminescent devices has become an urgent task. To realize the commercialization of full-color environmentally

friendly QLED technology, the performance of green InP-based devices still requires further effort by researchers. We demonstrated a strategy to *in-situ* passivate the InP cores, in which zinc myristate reacted with P dangling bonds to form Zn–P protective layer and protect InP cores from the water and oxygen in the environment. This proposed a safe and easy operating route for high-performance green InP-based devices.

Funding

Author contributions

F Chen, Z Wu and H Shen conceived and supervised the project. Y Cheng and Q Li contributed equally. Y Cheng and Q Li synthesized and characterized the materials. M Chen and F Chen fabricated and characterized the devices. All authors participated in the scientific discussion and the manuscript modification.

Conflict of interest

The authors declare that they have no competing financial interests.

ORCID iDs

Fei Chen ● https://orcid.org/0000-0003-0979-4276
Zhenghui Wu ● https://orcid.org/0000-0002-4187-9280

References

[1] Yadav R, Kwon Y, Rivaux C, Pierre C S, Ling W L and Reiss P 2023 Narrow near-infrared emission from InP QDs synthesized with indium (I) halides and aminophosphine *J. Am. Chem. Soc.* **145** 5970–81

[2] Dumbgen K C, Leemans J, De Roo V, Minjauw M, Detavernier C and Hens Z 2023 Surface chemistry of InP quantum dots, amine-halide co-passivation, and binding of Z-type ligands *Chem. Mater.* **35** 1037–46

[3] Zhou X, Ren J, Cao W, Meijerink A and Wang Y 2023 Narrow-band blue-emitting indium phosphide quantum dots induced by highly active Zn precursor *Adv. Opt. Mater.* **11** 2202128

[4] Lee Y, Jo D Y, Kim T, Jo J H, Park J, Yang H and Kim D 2022 Effectual interface and defect engineering for Auger recombination suppression in bright InP/ZnSeS/ZnS quantum dots *ACS Appl. Mater. Interfaces* **14** 12479–87

[5] Sung Y M *et al* 2021 Increasing the energy gap between band-edge and trap states slows down picosecond carrier trapping in highly luminescent InP/ZnSe/ZnS quantum dots *Small* **17** 2102792

[6] Dou Y, Wang L, Wang Y, Wu Q, Cao F, Wang S, Huang Q, Ma Y and Yang X 2023 Coordinating solvent synthesis of

[7] Shin S *et al* 2023 Fluoride-free synthesis strategy for luminescent InP cores and effective shelling processes via combinational precursor chemistry *Chem. Eng. J.* **466** 143223

[8] Huang P, Liu X, Jin G, Liu F, Shen H and Li H 2023 Deep-red InP core-multishell quantum dots for highly bright and efficient light-emitting diodes *Adv. Opt. Mater.* **11** 2300612

[9] Li H, Bian Y, Zhang W, Wu Z, Ahn T K, Shen H and Du Z 2022 High performance InP-based quantum dot light-emitting diodes via the suppression of field-enhanced electron delocalization *Adv. Funct. Mater.* **32** 2204529

[10] Won Y H, Cho O, Kim T, Chung D Y, Kim T, Chung H, Jang H, Lee J, Kim D and Jang E 2019 Highly efficient and stable InP/ZnSe/ZnS quantum dot light-emitting diodes *Nature* **575** 634–8

[11] Ubbink R F, Almeida G, Iziyi H, du Fossé I, Verkleij R, Ganapathy S, van Eck E R H and Houtepen A J 2022 A water-free in situ HF treatment for ultrabright InP quantum dots *Chem. Mater.* **34** 10093–103

[12] Fan X B *et al* 2023 InP/ZnS quantum dot photoluminescence modulation via in situ H$_2$S interface engineering *Nanoscale Horiz.* **8** 522–9

[13] Duan X, Ma J, Zhang W, Liu P, Liu H, Hao J, Wang K, Samuelson L and Sun X W 2023 Study of the interfacial oxidation of InP quantum dots synthesized from tris(dimethylamino)phosphine *ACS Appl. Mater. Interfaces* **15** 1619–28

[14] Li H, Zhang W, Bian Y, Ahn T K, Shen H and Ji B 2022 ZnF$_2$-assisted synthesis of highly luminescent InP/ZnSe/ZnS quantum dots for efficient and stable electroluminescence *Nano Lett.* **22** 4067–73

[15] Wang H C, Zhang H, Chen H Y, Yeh H C, Tseng M R, Chung R J, Chen S and Liu R S 2017 Cadmium-free InP/ZnSeS/ZnS heterostructure-based quantum dot light-emitting diodes with a ZnMgO electron transport layer and a brightness of over 10 000 cd m^{-2} *Small* **13** 1603962

[16] Zhang H *et al* 2019 High-efficiency green InP quantum dot-based electroluminescent device comprising thick-shell quantum dots *Adv. Opt. Mater.* **7** 1801602

[17] Moon H, Lee W, Kim J, Lee D, Cha S, Shin S and Chae H 2019 Composition-tailored ZnMgO nanoparticles for electron transport layers of highly efficient and bright InP-based quantum dot light emitting diodes *Chem. Commun.* **55** 13299–302

[18] Li Y, Hou X, Dai X, Yao Z, Lv L, Jin Y and Peng X 2019 Stoichiometry-controlled InP-based quantum dots: synthesis, photoluminescence, and electroluminescence *J. Am. Chem. Soc.* **141** 6448–52

[19] Chao W C, Chiang T H, Liu Y C, Huang Z X, Liao C C, Chu C H, Wang C H, Tseng H W, Hung W Y and Chou P T 2021 High efficiency green InP quantum dot light-emitting diodes by balancing electron and hole mobility *Commun. Mater.* **2** 96

[20] Zhang W *et al* 2022 High quantum yield blue InP/ZnS/ZnS quantum dots based on bromine passivation for efficient blue light-emitting diodes *Adv. Opt. Mater.* **10** 2200685

[21] Yu P, Cao S, Shan Y, Bi Y, Hu Y, Zeng R, Zou B, Wang Y and Zhao J 2022 Highly efficient green InP-based quantum dot light-emitting diodes regulated by inner alloyed shell component *Light Sci. Appl.* **11** 162

[22] Park J, Won Y H, Kim T, Jang E and Kim D 2020 Electrochemical charging effect on the optical properties of InP/ZnSe/ZnS quantum dots *Small* **16** 2003542

[23] Chen P, Liu H, Cui Y, Liu C, Li Y, Gao Y, Cheng J and He T 2023 Inner shell influence on the optical properties of

InP/ZnSeS/ZnS quantum dots *J. Phys. Chem.* C **127** 2464–70

[24] Okamoto A, Bai H, Toda S, Huang M, Kajii H, Kawai K and Murakami H 2023 Controlling thickness of ZnSe intermediate shell narrows FWHM of green-emitting spectra of InP/ZnSe/ZnS multi-shell quantum dots *ChemNanoMat* **9** e202200534

[25] Kim T G, Zherebetskyy D, Bekenstein Y, Oh M H, Wang L W, Jang E and Alivisatos A P 2018 Trap passivation in indium-based quantum dots through surface fluorination: mechanism and applications *ACS Nano* **12** 11529–40

[26] Zhang X, Hudson M H and Castellano F N 2021 Passivation of electron trap states in InP quantum dots with benzoic acid ligands *J. Phys. Chem.* C **125** 18362–71

[27] Pu Y C, Fan H C, Chang J C, Chen Y H and Tseng S W 2021 Effects of interfacial oxidative layer removal on charge carrier recombination dynamics in InP/ZnSe$_x$S$_{1-x}$ core/shell quantum dots *J. Phys. Chem. Lett.* **12** 7194–200

[28] Yang W, Yang Y, Kaledin A L, He S, Jin T, McBride J R and Lian T 2020 Surface passivation extends single and biexciton lifetimes of InP quantum dots *Chem. Sci.* **11** 5779–89

[29] Yoo D, Bak E, Ju H M, Shin Y M and Choi M J 2022 Zinc carboxylate surface passivation for enhanced optical properties of In(Zn)P colloidal quantum dots *Micromachines* **13** 1775

[30] Wu Q *et al* 2022 Quasi-shell-growth strategy achieves stable and efficient green InP quantum dot light-emitting diodes *Adv. Sci.* **9** 2200959

[31] Jo J H, Jo D Y, Choi S W, Lee S H, Kim H M, Yoon S Y, Kim Y, Han J N and Yang H 2021 Highly bright, narrow emissivity of InP quantum dots synthesized by aminophosphine: effects of double shelling scheme and Ga treatment *Adv. Opt. Mater.* **9** 2100427

[32] Taylor D A, Teku J A, Cho S, Chae W S, Jeong S J and Lee J S 2021 Importance of surface functionalization and purification for narrow FWHM and bright green-emitting InP core-multishell quantum dots via a two-step growth process *Chem. Mater.* **33** 4399–407

[33] Xu H *et al* 2024 Dipole-dipole-interaction-assisted self-assembly of quantum dots for highly efficient light-emitting diodes *Nat. Photon.* **18** 186–91

[34] Deng Y *et al* 2022 Solution-processed green and blue quantum-dot light-emitting diodes with eliminated charge leakage *Nat. Photon.* **16** 505–11

[35] Han C Y, Lee S H, Song S W, Yoon S Y, Jo J H, Jo D Y, Kim H M, Lee B J, Kim H S and Yang H 2020 More than 9% efficient ZnSeTe quantum dot-based blue electroluminescent devices *ACS Energy Lett.* **5** 1568–76

[36] Zhang T *et al* 2023 Electric dipole modulation for boosting carrier recombination in green InP QLEDs under strong electron injection *Nanoscale Adv.* **5** 385–92

[37] Kim J, Hong A, Hahm D, Lee H, Bae W K, Lee T and Kwak J 2023 Realization of highly efficient InP quantum dot light-emitting diodes through in-depth investigation of exciton-harvesting layers *Adv. Opt. Mater.* **11** 2300088